Impact of sulfur addition on the structure and dynamics of Ni–Nb alloy melts

Nicolai Grund ; Dirk Holland-Moritz ; Saba Khademorezaian ; Lucas P. Kreuzer ; Nico Neuber ;
Lucas M. Ruschel ; Hendrik Voigt; Johanna Wilden ; Fan Yang ✉ ; Soham Banerjee;
Malte Blankenburg ; Ann-Christin Dippel ; Jan Peter Embs ; Sergiy Divinski ; Ralf Busch;
Andreas Meyer ; Gerhard Wilde

Check for updates

View Online   Export Citation

Impact of sulfur addition on the structure and dynamics of Ni–Nb alloy melts

Nicolai Grund,[1] (ID) Dirk Holland-Moritz,[1] (ID) Saba Khademorezaian,[2] (ID) Lucas P. Kreuzer,[1,3] (ID) Nico Neuber,[4] (ID) Lucas M. Ruschel,[4] (ID) Hendrik Voigt,[2] Johanna Wilden,[1] (ID) Fan Yang,[1,a)] (ID) Soham Banerjee,[5] Malte Blankenburg,[5] Ann-Christin Dippel,[5] (ID) Jan Peter Embs,[6] (ID) Sergiy Divinski,[2] (ID) Ralf Busch,[4] Andreas Meyer,[1] (ID) and Gerhard Wilde[2] (ID)

AFFILIATIONS

[1] Institut für Materialphysik im Weltraum, Deutsches Zentrum für Luft- und Raumfahrt (DLR), 51170 Köln, Germany
[2] Institute of Materials Physics, University of Münster, 48149 Münster, Germany
[3] Heinz Maier-Leibnitz-Zentrum, Technische Universität München, Lichtenbergstraße 1, 85748 Garching, Germany
[4] Chair of Metallic Materials, Saarland University, 66123 Saarbrücken, Germany
[5] Deutsches Elektronen-Synchrotron DESY, Notkestraße 85, 22607 Hamburg, Germany
[6] Paul Scherrer Institut, Forschungsstrasse 111, 5232 Villigen, Switzerland

[a)] Author to whom correspondence should be addressed: fan.yang@dlr.de

ABSTRACT

We investigated the change in the structure and dynamics of a Ni–Nb bulk metallic glass upon sulfur addition on both microscopic and macroscopic scales. With the sulfur concentration of 3 at. %, where the composition $Ni_{58}Nb_{39}S_3$ exhibits the best glass forming ability in the investigated sulfur concentration range, both the equilibrium and undercooled melt dynamics remain almost unchanged. Only in the glassy state does sulfur seem to result in mass transport less decoupled to the viscosity of the undercooled liquid, where the measured Ag tracer diffusion coefficient is slower in the ternary alloy. With the structural disorder introduced by the alloying sulfur, the improved glass forming ability is attributed to geometrical frustration, where crystal nucleation requires a depletion of sulfur and hence long range diffusion, as long as no primary sulfur-containing crystalline phase is involved.

The properties of many alloys can be fundamentally changed by adding a minor amount of additional elements. Such ways of incorporating alloy elements are sometimes also referred to as micro-alloying, if the concentration of additives is at a very low level. For bulk metallic glasses (BMGs), minor- or micro-alloying have often been applied to improve their properties with respect to strength, hardness, elasticity, plasticity, and glass-forming ability.[1–4]

Ni–Nb based BMGs belong to the best glass forming alloys already in the binary system. The $Ni_{62}Nb_{38}$ composition exhibits a high glass forming ability (GFA), allowing a vitreous casting thickness of 2 mm.[5] The achievable strength can be as high as 3 GPa, with the Vickers hardness of 860 HV5.[6] Moreover, the combination of a large elastic limit of 2% and a high glass transition temperature makes them particularly interesting for engineering-oriented applications. Therefore, the binary alloy system has been often fine-tuned using minor- or micro-alloying, conventionally by adding metallic elements, such as Sn, Zr, and Ta.[7–9]

In contrast to these metallic elements, just recently, using metalloid elements, such as P and S, as alloying components has been shown to be highly beneficial for glass formation and thermal stability. While P has also been used as an alloying element for Pd- or Fe-based BMGs, particularly sulfur as an alloying element has not been widely used before for BMGs, despite its wide availability in various industrial processes. Since then, it has been found that sulfur addition improves the GFA of various BMGs, including several Pd-, Ti-, Zr-, and Cu-based alloy systems.[10–13]

However, the influence of sulfur on the structure and dynamics of the alloy melts/glasses has not been fully understood until now. One possible effect of the minor alloying is the alternation in the liquid behavior from a kinetically fragile to kinetically stronger behavior. This causes a decrease in the atomic mobility above the glass transition temperature T_g, delaying the crystallization process, which ultimately enhances the GFA. Another possibility is the alternation of the primary precipitating phases, preventing the formation of crystalline species that compete with the liquid phase. So far, only a limited number of ternary alloys have been investigated. In Ti–Ni–S-based alloys, a more sluggish liquid dynamics upon a sulfur addition in the range of 5–8 at. % has indeed been observed, whereas in the Pd–Ni–S alloy melts, where the sulfur content is considerably higher, the diffusive dynamics of Ni depends only very weakly on the sulfur concentration.[14,15] This indicates that the mechanisms of improved GFA upon sulfur addition can be different in different alloy systems.

Sulfur addition improves the GFA of the $Ni_{62}Nb_{38}$ alloy at even lower sulfur concentrations compared to the case of Ti–Ni–S. The best glass forming composition has been found at about 3 at. % sulfur addition, at the composition $Ni_{58}Nb_{39}S_3$ (3 mm critical casting thickness). Further increases in the sulfur content deteriorate the GFA of the alloy (see the supplementary material). Thus, the Ni–Nb–S alloy system represents a typical case of minor addition. In the following, we present the results on the change of structure and dynamics of these melts/glasses upon sulfur addition. By using particular advanced scattering and diffraction techniques, we are able to access these properties on both microscopic and macroscopic scales, in order to reveal the mechanisms of the improved GFA.

The $Ni_{62}Nb_{38}$ master alloy was produced from the high-purity raw materials, Ni (99.99 wt. %) and Nb (99.95 wt. %), under a Ti-gettered high-purity Ar atmosphere. For the alloy $Ni_{58}Nb_{39}S_3$, an inductively synthesized $Ni_{55}S_{45}$ (in at. %) pre-alloy (S 99.9995 wt. %) was additionally used. The detailed production procedure is provided in Ref. 9. The amorphous specimens were prepared by subsequent suction casting into water-cooled Cu molds. Their glassy structure was verified by x-ray diffraction (XRD) and further characterized by differential scanning calorimetry (DSC). The viscosity of the metastable undercooled liquid close to T_g was measured in a Netzsch TMA 402 F3 Hyperion thermo-mechanical analyzer (TMA) using a three-point bending setup with rectangular beam-shaped specimens. This provides high accuracy in the high viscosity range of 10^8–10^{15} Pa s.[16] To determine the equilibrium viscosity below the calorimetric glass transition temperature, isothermal measurements were conducted. The sample undergoes a relaxation process from the glassy state into the supercooled liquid, where the viscosity of the metastable equilibrium liquid is determined by the long-time limiting value. For measurements above the calorimetric glass transition, a scan protocol was used, where the viscosity was determined upon entering the deeply supercooled liquid state. This allows the determination of viscosity in the supercooled liquid region up to the onset of crystallization. In particular, for $Ni_{62}Nb_{38}$, the low temperature viscosity was only measured during heating.

High temperature viscosity of the $Ni_{62}Nb_{38}$ and $Ni_{58}Nb_{39}S_3$ alloys were measured employing an oscillating drop technique,[17] where a droplet of the sample is levitated in order to avoid any possible contamination. A surface oscillation is excited before the measurement. Its characteristic decay time after switching off the excitation is then used to derive the melt viscosity. The $Ni_{62}Nb_{38}$ samples were processed using electrostatic levitation.[18] The $Ni_{58}Nb_{39}S_3$ sample was processed under reduced gravity conditions on the board of the TEMPUS parabolic flight facility using electromagnetic levitation,[19] owing to the fact that it was necessary to heat the sample to temperatures 200–300 K above their liquidus temperature to fully dissolve sulfur, which is not possible in electrostatic levitation for the duration of the viscosity measurement due to evaporation.

The Ni self-diffusion coefficients in the melt were measured using quasielastic neutron scattering (QENS) on the FOCUS instrument located at the Swiss Spallation Neutron Source. An incoming neutron wavelength of 4.4 Å was chosen, which gives an instrumental energy resolution of about 100 μeV. The samples were processed in thin-walled Al_2O_3 containers, with a diameter of 5 mm and a height of about 30 mm. QENS probes the dynamics of the melt on microscopic time and length scales, allowing accurate determination of the Ni self-diffusion coefficient, free of any convective artifacts.[20] The measurements were performed at four different temperatures between 1573 and 1693 K for both the alloy compositions. Dynamic structure factors $S(q, \omega)$ were obtained for each sample and temperature after normalization of the measured intensity to a vanadium standard, subtraction of the empty cell contribution, angular correction for self-absorption and container absorption, conversion from the neutron time-of-flight to energy transfer, and interpolation to constant momentum transfers q. Then, $S(q, \omega)$ can be described by a single Lorentzian function, where the Ni self-diffusion coefficient is derived from the q dependent half width at half maximum in the range $0.5 < q < 1.2$ Å^{-1}, where incoherent scattering is dominant.

The impact of sulfur alloying on the diffusion rates in the glass was evaluated using Ag as a tracer element. A thin, 10–20 nm thick, layer of natural Ag was deposited onto polished cuboid-shaped samples with sizes of about $3 \times 3 \times 0.3$ mm^3 using a magnetron sputtering device. The Ag tracer was selected to enable accurate measurements of diffusion kinetics by time-of-flight secondary ion mass spectrometry (ToF-SIMS) without interference from the elements constituting the glasses. Diffusion annealing treatments were carried out in sealed quartz tubes under purified (5N) argon atmosphere. After annealing the Ag concentration, the profiles were analyzed using an IONTOF ToF-SIMS 5–300 device. The areas of 300×300 μm^2 were typically sputtered from which pore- and defect-free areas of 100×100 μm^2 were selected for the final analysis, from which the tracer diffusion coefficients were evaluated from the broadening of the Gaussian-type branches. For example, see Ref. 21 for further details.

The total structure factors of the liquids were measured by high energy XRD at DESY. Samples with diameters of about 3 mm were processed in an electrostatic levitation apparatus adapted for scattering experiments.[22] A monochromatic x-ray beam with a size of about 1×1 mm^2 and an energy of ~100 keV was used. The diffraction experiments were performed in transmission geometry. The 2D scattering intensity was collected using a flat-panel detector, from which 1D diffraction patterns were calculated using the pyFAI software package.[23] The structure factor of the liquid was then derived from the integrated intensity using pdfgetX2 software,[24] with the procedures described in Ref. 25.

Structural investigation on the medium range order (MRO) scale was done using variable resolution fluctuation electron microscopy (vR FEM) in a ThermoFisher Scientific Themis 300 G3 transmission electron microscope (TEM). The spatial fluctuations in the diffracted intensity, expressed in the normalized variance $V(\vec{k}, R)$ = $\frac{\langle I^2(\vec{k},R,\vec{r})\rangle}{\langle I(\vec{k},R,\vec{r})\rangle^2} - 1$ of nano-sized volumes was extracted from the measured nanobeam diffraction patterns (NBDPs),[1,26,27] with $\langle \rangle$ being the average over the sample position $\vec{r}$. In the experiment, a parallel coherent probe with a full width at half maximum (FWHM) between 0.8 and 7.7 nm is scanned over the sample. For each normalized variance curve, 100 NBDP were acquired on a 50×50 nm^2 region with a beam current of 10 pA, an exposure time of 4 s, a camera length of 77 nm, and binning 4. During the measurement, it was ensured that the thickness was kept constant at $t/\lambda = 0.65$ for all the measurements and sample systems to ensure comparability. In a so-called Stratton–Voyles plot, the normalized variance peak maximum is plotted against $1/R^2$, which gives information on the MRO length scale and the MRO volume fraction.[28–30] The detected MRO correlation lengths are typically in the range of 1–6 nm.[1,26,31,32]

The high and low temperature viscosity of the binary $Ni_{62}Nb_{38}$ and the ternary $Ni_{58}Nb_{39}S_3$ alloys are shown in Fig. 1. The data are shown as a function of scaled temperature T_g/T, where
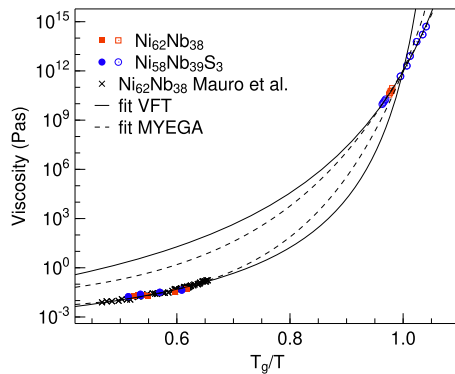
FIG. 1. High (close to the liquidus temperature and closed symbols) and low (close to T_g and open symbols) temperature viscosity of the $Ni_{62}Nb_{38}$ and $Ni_{58}Nb_{39}S_3$ alloys, shown on the reduced temperature scale T_g/T. The solid lines are fitted according to the VFT model, and the dashed lines are indicating the use of the MYEGA model.
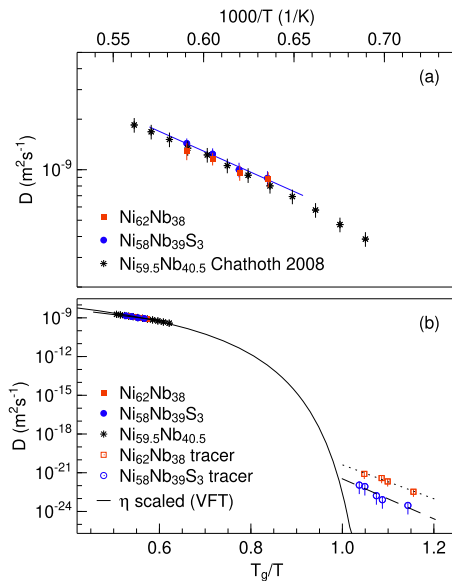
T_g is defined as the viscosity $\eta(T_g) = 10^{12}$ Pa s. This corresponds to 901 K for $Ni_{62}Nb_{38}$ and 892 K for the $Ni_{58}Nb_{39}S_3$ alloy. The temperature dependence of the melt viscosity is described by two different models using (1) the Vogel–Fulcher–Tammann (VFT) equation:[33] $\eta(T) = \eta_0 \exp\left(\frac{D^* T_0}{T - T_0}\right)$, with the fragility parameter D^*, the VFT temperature T_0, and the pre-exponential factor η_0, and (2) the Mauro–Yue–Ellison–Gupta–Allan (MYEGA) equation,[34] $\eta(T) = \eta_0 \exp\left[\frac{K}{T} \exp\left(\frac{H}{T}\right)\right]$, with the pre-exponential factor η_0 and the fitting parameters K and H. For binary $Ni_{62}Nb_{38}$, the high temperature viscosity measured in ESL is in agreement with that measured by Mauro et al.[35] within the experimental uncertainty, which are included for fitting the temperature dependence of the melt viscosity. For both the models, over the entire temperature range studied, the viscosity data cannot be described by a single set of parameters, which is known also for many other metallic glass forming alloys.[36,37] However, it can be recognized from Fig. 1 that in both the high and low temperature regimes, the viscosities of the binary and the sulfur containing alloys falls on the same fitting curve. The fitting parameters obtained are slightly different for the binary and the sulfur containing melts, which is mainly due to the different temperature ranges covered. The obtained D^* are similar for the two alloys (Table I).

Figure 2(a) shows the Ni self-diffusion coefficients of the equilibrium melts of the $Ni_{62}Nb_{38}$ and the $Ni_{58}Nb_{39}S_3$ alloys measured in the temperature range between 1573 and 1693 K by QENS. The solid line represents an Arrhenius fit of the Ni self-diffusion rates in the $Ni_{58}Nb_{39}S_3$ melt, which gives an activation energy $E_A = 944 \pm 80$ meV. The activation energy obtained for the Ni diffusion in the $Ni_{62}Nb_{38}$ is 775 ± 79 meV. In Fig. 2(a), the values of the measured self-diffusion coefficients are compared to those of the eutectic $Ni_{59.5}Nb_{40.5}$ alloy,[38] which agree with the off-eutectic and the sulfur containing alloys within the experimental uncertainties.

Similar to the Ti–Ni–S alloys, the Ni–Nb–S alloy contains an early transition metal and Ni. In the Ti–Ni–S melt, the melt dynamics slow down with increasing sulfur content, as a result of potential covalent-like interactions involved.[14] Despite the chemical similarity (e.g., Ti–Nb forms a completely miscible binary phase diagram[39]), the melt dynamics does not seems to be affected by the sulfur addition for $Ni_{58}Nb_{39}S_3$. However, a distinct difference is that overall the sulfur concentration in the studied Ti–Ni–S alloys is higher, in the range of 5 – 8 at. %, whereas for the Ni–Nb–S alloys, the optimized GFA is already found in the range between 1 and 3 at. % sulfur addition. As it is already suggested for the Ti–Ni–S alloys that sulfur

TABLE I. Fit parameters obtained on the measured viscosities of the $Ni_{62}Nb_{38}$ and $Ni_{58}Nb_{39}S_3$ alloys using the VFT and MYEGA equations for the high temperature (HT) and low temperature (LT) branches.

Composition	$\ln \eta_0$ (ln Pas)	$D^{*,HT}$	T_0^{HT} (K)	$D^{*,LT}$	T_0^{LT} (K)
$Ni_{62}Nb_{38}$	-8.08 ± 0.10	4.4 ± 0.1	801 ± 2	12.1 ± 0.4	674 ± 7
$Ni_{58}Nb_{39}S_3$	-5.94 ± 0.40	2.1 ± 0.4	839 ± 9	10.6 ± 0.1	678 ± 1
		K^{HT}	H^{HT}	K^{LT}	H^{LT}
$Ni_{62}Nb_{38}$	-6.03 ± 0.07	111 ± 6	4305 ± 47	636 ± 67	2731 ± 98
$Ni_{58}Nb_{39}S_3$	-4.74 ± 0.26	22 ± 11	5647 ± 458	459 ± 8	2951 ± 16

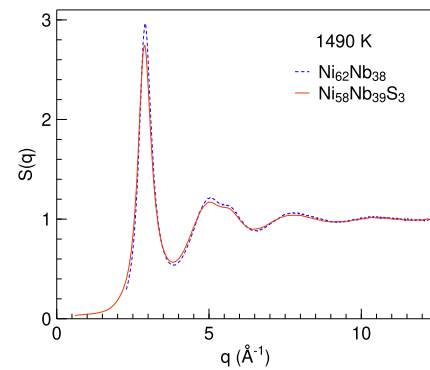FIG. 3. Total x-ray structure factor of the $Ni_{62}Nb_{38}$ and $Ni_{58}Nb_{39}S_3$ alloys measured by x-ray diffraction at 1490 K. The measurement of the binary alloy was performed using a combined SAXS/WAXS setup where the access to lower q is more limited.

FIG. 2. (a) Comparison of the Ni self-diffusion coefficient measured by QENS for the $Ni_{62}Nb_{38}$ (closed square) and $Ni_{58}Nb_{39}S_3$ (closed circle) melts. Data are compared to that of the eutectic $Ni_{59.5}Nb_{40.5}$ alloy.[38] The blue solid line is an Arrhenius fit of the Ni self-diffusion coefficient of the $Ni_{58}Nb_{39}S_3$ alloy. (b) Scaled diffusion data for both alloys according to the $\eta(T_g) = 10^{12}$ Pa s, together with the measured Ag tracer diffusion coefficients. The solid line represents the scaled diffusivity of the high temperature VFT fit of the melt viscosity (see the text).

may introduce a unique melt structure, in the following, we present the structural results of both the liquid and the glass.

Figure 2(b) shows the temperature-dependent self-diffusion coefficients, plotted in the T_g/T scale together with the low temperature Ag tracer diffusion coefficients. The high temperature Ni self-diffusion coefficients of the binary and ternary alloys fall on top of each other, showing similar temperature dependence. At temperatures below T_g, the Ag diffusion coefficient of the binary and ternary alloys are different, where the sulfur-containing alloy exhibits lower diffusion coefficients. In the temperature interval under investigation, the activation energies are determined to be 995 ± 8 meV and 1161 ± 10 meV for $Ni_{62}Nb_{38}$ and $Ni_{58}Nb_{39}S_3$, respectively. While practically sulfur does not influence the Ni self-diffusion rates in the liquid state, it seems that its alloying retards Ag diffusion in the glassy state.

When compared to the scaled melt viscosity according to $D(T) = 2.53 \times 10^{-11}/\eta(T)$,[40] where the high temperature VFT-fit represents the upper limit of the scaled diffusivity, it can be seen that the Ag tracer diffusion, i.e., of an impurity in the glass, is still faster. It is well-known that the diffusion coefficient of some species decouples from the scaled viscosity in the undercooled liquid state of multicomponent alloys, particularly in the range of the glass transition.[41,42] Thus, such deviations can be expected. In our case, it seems that for $Ni_{58}Nb_{39}S_3$, the Ag diffusion below the glass transition temperature is more strongly coupled to the liquid viscosity compared to the case of $Ni_{62}Nb_{38}$.

Figure 3 shows the measured x-ray total structure factor of the $Ni_{62}Nb_{38}$ and $Ni_{58}Nb_{39}S_3$ alloys at 1490 K. It can be seen that

the position of the first structure factor maximum of the ternary $Ni_{58}Nb_{39}S_3$ melt shifts slightly from $q = 2.910 \pm 0.005$ Å^{-1} of the binary alloy to $q = 2.879 \pm 0.016$ Å^{-1}. This difference could be accounted by the slightly different Ni/Nb ratio, if structure factors of the Ni–S or Nb–S isomorphic substitutions are calculated using the available partial structure factors of the binary $Ni_{59.5}Nb_{40.5}$ melt.[43] In contrast, the reduced peak amplitude cannot be explained by both the isomorphic substitutions.

Figure 4 shows a Stratton–Volyes plot obtained by FEM on the $Ni_{62}Nb_{38}$ and $Ni_{58}Nb_{39}S_3$ alloys in the glass state. A peak or plateau indicates that the MRO length scale is matching the size of the probe used. It can be seen that the peak position is very similar for the binary and ternary samples. From the normalized variance curves, the position of the first peak was determined to be between 4 and 5.5 nm^{-1}. The mean position of the first peak that was determined by fitting a Gaussian fit gives 4.86 ± 0.03 nm^{-1} for the $Ni_{62}Nb_{38}$ alloy and 4.88 ± 0.03 nm^{-1} for the $Ni_{58}Nb_{39}S_3$ alloy, indicating that the underlying MRO is on the same length scale. Furthermore, the MRO volume fraction can be semi-quantitatively estimated from the height of the normalized variance peaks.[1,32,44] The absolute peak height was measured at $V_{max} = 0.199$ for $Ni_{62}Nb_{38}$ and $V_{max} = 0.173$ for $Ni_{58}Nb_{39}S_3$, which implies a slightly higher MRO volume fraction, on the order of 20%, of the binary alloy. This is in line with the observed decrease in the amplitude of the first diffraction peak of the liquid $S(q)$, indicating that the sulfur addition introduces more disorder on the scale of both interatomic distances and MRO. However, overall the differences are rather small, which is most probably due to the small sulfur addition that leads to a rather uniform spatial distribution of the more covalent/directional bonds. In fact, with the sulfur containing alloy presenting a rather similar MRO type, fraction, and specific volume, a more coupled diffusivity at temperatures close to T_g, as experimentally observed for the sulfur containing system with more covalent bonding character, would be expected and is in line with the observed increased critical casting thickness of the sulfur containing alloy.[45,46]

Elementary sulfur is known for its complex coordination behavior and forms more allotropes than any other element. Conceptually, it may be expected that adding sulfur to a metallic melt considerably increases the topological variability and complexity. In
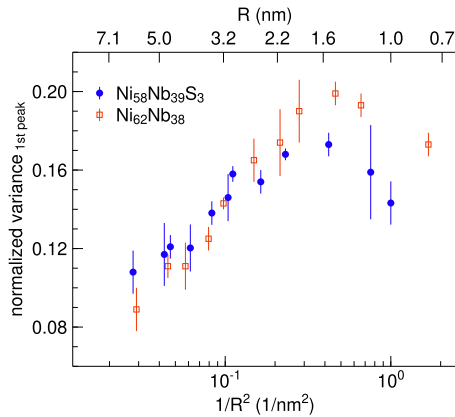
FIG. 4. FEM analysis visualized in the form of Stratton–Voyles plots, i.e., peak height at the first maximum in the normalized variance curves plotted against $1/R^2$, shown for the $Ni_{62}Nb_{38}$ and $Ni_{58}Nb_{39}S_3$ glasses.

particular, the covalent contributions of the interatomic interaction potential between sulfur and other elements promotes geometrical frustration. This is also known as a concept to improve GFA of metallic melts via increasing the number of alloy elements, ideally with different atomic sizes, which are more difficult to be incorporated in possible crystal structures.

In fact, the crystallization behavior of the $Ni_{58}Nb_{39}S_3$ alloy from the levitated melt observed in the time-resolved synchrotron diffraction experiment shows that no sulfur-containing compound is involved as primary phases upon solidification, as shown in the upper panel of Fig. 5. The Bragg reflections observed are identical to those observed in the binary $Ni_{62}Nb_{38}$ alloy under similar conditions,[9] which match to those of Ni_3Nb and Ni_6Nb_7. In contrast, in the case of $(Ni_{62}Nb_{38})_{95}S_5$, solidification of a different initial phase
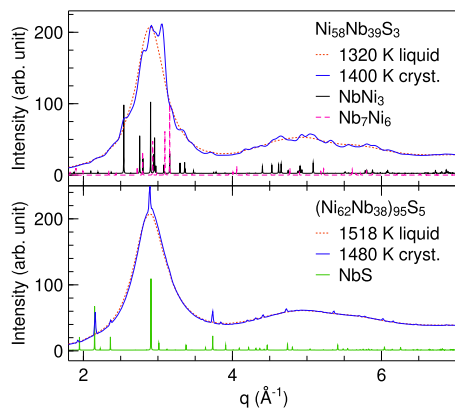
FIG. 5. Diffractograms obtained during cooling of the melts prior to crystallization and of the initial phases formed during the solidification of $Ni_{58}Nb_{39}S_3$ and $(Ni_{62}Nb_{38})_{95}S_5$ alloys, observed in time-resolved synchrotron diffraction experiments employing levitation. In the case of $Ni_{58}Nb_{39}S_3$, no primary sulfur-containing phase is observed, whereas the initial phase formed in the case of $(Ni_{62}Nb_{38})_{95}S_5$ is NbS. The small shift in the position of the observed diffraction peaks can be attributed to thermal expansions.

is observed, which is identified as NbS,[47] as shown in the lower panel of Fig. 5. Thus, for $Ni_{58}Nb_{39}S_3$, crystal nucleation requires long range diffusion of constituents, particularly the exclusion of sulfur.[48,49] The very weak changes of both the dynamics and the thermodynamic properties such as liquidus temperatures of the Ni–Nb melt, at a sulfur alloying level as low as 3 at. %, indicates the likeliness of such a mechanism to enhance GFA, whereas the formation of primary sulfur-containing phases at 5 at. % sulfur addition seems to deteriorate the GFA.

In summary, we studied the change in the structure and dynamics of the Ni–Nb stable and undercooled melt and the glass upon alloying 3 at. % sulfur, which exhibits the best combination of GFA and thermal stability in the sulfur concentration range up to 5 at. %. The ternary $Ni_{58}Nb_{39}S_3$ alloy exhibits very similar melt dynamics when compared to the binary $Ni_{62}Nb_{38}$, whereas the ternary alloy seems to show more structural disorder. The enhanced GFA is attributed to a geometrical frustration upon sulfur addition, where incorporation of sulfur in the initial crystalline phases is hindered. These results shed new light on the remarkable efficiency of minor alloying to enhance the GFA of metallic alloys, as at both the nucleation and/or growth stages, vitrification are highly sensitive to atomic mobility and to the distribution of motifs.

The supplementary material contains the compositional dependence of the critical casting thickness d_c as well as of the thermal stability of the undercooled liquid region ΔT_x upon heating above the glass transition temperature for various Ni–Nb–S alloys. This also covers a variation of the Ni/Nb ratio at a sulfur concentration of 3 at. %.

AUTHOR DECLARATIONS

Conflict of Interest

The authors have no conflicts to disclose.

Author Contributions

Nicolai Grund: Data curation (equal); Formal analysis (equal); Investigation (equal). **Dirk Holland-Moritz**: Data curation (equal); Formal analysis (equal); Investigation (equal); Validation (equal); Writing – review & editing (equal). **Saba Khademorezaian**: Data curation (equal); Formal analysis (equal); Investigation (equal); Validation (equal); Writing – review & editing (equal). **Lucas P. Kreuzer**: Data curation (equal); Investigation (equal); Writing – review & editing (equal). **Nico Neuber**: Data curation (equal); Formal analysis (equal); Investigation (equal); Validation (equal). **Lucas M. Ruschel**: Data curation (equal); Formal analysis (equal); Investigation (equal); Validation (equal); Writing – review & editing (equal). **Hendrik Voigt**: Data curation (equal); Formal analysis (equal); Investigation (equal); Validation (equal); Writing –

02 June 2024 17:21:06

DATA AVAILABILITY

The data that support the findings of this study are available from the corresponding author upon reasonable request.

REFERENCES

[1] S. Hilke, H. Rösner, and G. Wilde, "The role of minor alloying in the plasticity of bulk metallic glasses," Scr. Mater. **188**, 50–53 (2020).

[2] W. H. Wang, "Roles of minor additions in formation and properties of bulk metallic glasses," Prog. Mater. Sci. **52**, 540–596 (2007).

[3] Z. P. Lu and C. T. Liu, "Role of minor alloying additions in formation of bulk metallic glasses: A review," J. Mater. Sci. **39**, 3965–3974 (2004).

[4] N. Nollmann, I. Binkowski, V. Schmidt, H. Rösner, and G. Wilde, "Impact of micro-alloying on the plasticity of pd-based bulk metallic glasses," Scr. Mater. **111**, 119–122 (2016), part of Special Issue viewpoint Set No. 57: Contemporary Innovations for Thermoelectrics Research and Development.

[5] L. Xia, W. H. Li, S. S. Fang, B. C. Wei, and Y. D. Dong, "Binary Ni–Nb bulk metallic glasses," J. Appl. Phys. **99**, 026103 (2006).

[6] Z. Zhu, H. Zhang, D. Pan, W. Sun, and Z. Hu, "Fabrication of binary Ni–Nb bulk metallic glass with high strength and compressive plasticity," Adv. Eng. Mater. **8**, 953–957 (2006).

[7] Z. Zhu, H. Zhang, B. Ding, and Z. Hu, "Synthesis and properties of bulk metallic glasses in the ternary Ni–Nb–Zr alloy system," Mater. Sci. Eng.: A **492**, 221–229 (2008).

[8] D. Li, H. Zhang, A. Wang, Z. Zhu, and Z. Hu, "Effect of Sn addition on the glass-forming ability and mechanical properties of Ni–Nb–Zr bulk metallic glasses," Chin. Sci. Bull. **56**, 3926–3931 (2011).

[9] L. M. Ruschel, O. Gross, B. Bochtler, B. Li, B. Adam, N. Neuber, M. Frey, S. Jakovlev, F. Yang, H.-R. Jiang, B. Gludovatz, J. J. Kruzic, and R. Busch, "Ni–Nb–P-based bulk glass-forming alloys: Superior material properties combined in one alloy family," Acta Mater. **253**, 118968 (2023).

[10] A. Kuball, B. Bochtler, O. Gross, V. Pacheco, M. Stolpe, S. Hechler, and R. Busch, "On the bulk glass formation in the ternary Pd–Ni–S system," Acta Mater. **158**, 13–22 (2018).

[11] A. Kuball, O. Gross, B. Bochtler, and R. Busch, "Sulfur-bearing metallic glasses: A new family of bulk glass-forming alloys," Scr. Mater. **146**, 73–76 (2018).

[12] A. Kuball, O. Gross, B. Bochtler, B. Adam, L. Ruschel, M. Zamanzade, and R. Busch, "Development and characterization of titanium-based bulk metallic glasses," J. Alloys Compd. **790**, 337–346 (2019).

[13] O. Gross, L. Ruschel, A. Kuball, B. Bochtler, B. Adam, and R. Busch, "Bulk metallic glass formation in the (Ti, Zr)–(Ni, Cu)–S system," J. Phys. Condens. Matter **32**, 264003 (2020).

[14] J. Wilden, F. Yang, D. Holland-Moritz, S. Szabó, W. Lohstroh, B. Bochtler, R. Busch, and A. Meyer, "Impact of sulfur on the melt dynamics of glass forming $Ti_{75}Ni_{25-x}S_x$," Appl. Phys. Lett. **117**, 013702 (2020).

[15] J. Wilden, F. Yang, G. Günther, M. Russina, A. Kuball, R. Busch, and A. Meyer, "Ni self-diffusion in glass forming Pd–Ni–S melts," J. Phys. Condens. Matter **33**, 435101 (2021).

[16] H. E. Hagy, "Experimental evaluation of beam-bending method of determining glass viscosities in the range 10^8 to 10^{15} poises," J. Am. Ceram. Soc. **46**, 93–97 (1963).

[17] W.-K. Rhim, K. Ohsaka, P.-F. Paradis, and R. E. Spjut, "Noncontact technique for measuring surface tension and viscosity of molten materials using high temperature electrostatic levitation," Rev. Sci. Instrum. **70**, 2796–2801 (1999).

[18] P. Heintzmann, F. Yang, S. Schneider, G. Lohöfer, and A. Meyer, "Viscosity measurements of metallic melts using the oscillating drop technique," Appl. Phys. Lett. **108**, 241908 (2016).

[19] T. Tempus, "Containerless processing in space: Recent results," in *Materials and Fluids Under Low Gravity*, edited by L. Ratke, H. Walter and B. Feuerbacher (Springer Berlin Heidelberg, Berlin Heidelberg, 1996), pp. 233–252.

[20] A. Meyer, "The measurement of self-diffusion coefficients in liquid metals with quasielastic neutron scattering," EPJ Web Conf. **83**, 01002 (2015).

[21] D. Gärtner, L. Belkacemi, V. A. Esin, F. Jomard, A. A. Fedotov, J. Schell, J. V. Osinskaya, A. V. Pokoev, C. Duhamel, A. Paul, and S. V. Divinski, "Techniques of tracer diffusion measurements in metals, alloys and compounds," Diffus. Found. **29**, 31–73 (2021).

[22] T. Kordel, D. Holland-Moritz, F. Yang, J. Peters, T. Unruh, T. Hansen, and A. Meyer, "Neutron scattering experiments on liquid droplets using electrostatic levitation," Phys. Rev. B **83**, 104205 (2011).

[23] G. Ashiotis, A. Deschildre, Z. Nawaz, J. P. Wright, D. Karkoulis, F. E. Picca, and J. Kieffer, "The fast azimuthal integration Python library: *pyFAI*," J. Appl. Crystallogr. **48**, 510–519 (2015).

[24] X. Qiu, J. W. Thompson, and S. J. L. Billinge, "*PDFgetX2*: A GUI-driven program to obtain the pair distribution function from X-ray powder diffraction data," J. Appl. Crystallogr. **37**, 678 (2004).

[25] M. Ruiz-Martín, D. Holland-Moritz, F. Yang, C. Yuan, G. Simeoni, T. Hansen, U. Rütt, O. Gutowski, J. Bednarčík, and A. Meyer, "Microscopic structure and dynamics of glass forming Zr_2Co melts and the impact of different late transition metals on the melt properties," J. Non-Cryst. Solids: X **16**, 100131 (2022).

[26] P. Voyles and D. Muller, "Fluctuation microscopy in the STEM," Ultramicroscopy **93**, 147–159 (2002).

[27] S. Hilke, H. Rösner, D. Geissler, A. Gebert, M. Peterlechner, and G. Wilde, "The influence of deformation on the medium-range order of a Zr-based bulk metallic glass characterized by variable resolution fluctuation electron microscopy," Acta Mater. **171**, 275–281 (2019).

[28] M. Treacy and J. Gibson, "Variable coherence microscopy: A rich source of structural information from disordered materials," Acta Crystallogr., Sect. A: Found. Crystallogr. **52**, 212–220 (1996).

[29] P. Voyles, J. Gibson, and M. Treacy, "Fluctuation microscopy: A probe of atomic correlations in disordered materials," J. Electron Microsc. **49**, 259–266 (2000).

[30] W. Stratton and P. Voyles, "A phenomenological model of fluctuation electron microscopy for a nanocrystal/amorphous composite," Ultramicroscopy **108**, 727–736 (2008).

[31] R. Dash, P. Voyles, J. Gibson, M. Treacy, and P. Keblinski, "A quantitative measure of medium-range order in amorphous materials from transmission electron micrographs," J. Phys. Condens. Matter **15**, S2425 (2003).

[32] S. Bogle, L. Nittala, R. Twesten, P. Voyles, and J. Abelson, "Size analysis of nanoscale order in amorphous materials by variable-resolution fluctuation electron microscopy," Ultramicroscopy **110**, 1273–1278 (2010).

[33] H. Vogel, "Das temperaturabhaengigkeitsgesetz der viskositaet von fluessigkeiten," Z. Phys **22**, 645–646 (1921). G. S. Fulcher, "Analysis of

recent measurements of the viscosity of glasses," J. Am. Ceram. Soc. **8**, 339–355 (1925). G. Tammann, and W. Hesse, "Die abhängigkeit der viscosität von der temperatur bie unterkühlten flüssigkeiten," Z. Anorg. Allg. Chem. **156**, 245–257 (1926).

[34] J. C. Mauro, Y. Yue, A. J. Ellison, P. K. Gupta, and D. C. Allan, "Viscosity of glass-forming liquids," Proc. Natl. Acad. Sci. U. S. A. **106**, 19780–19784 (2009).

[35] N. A. Mauro, M. Blodgett, M. L. Johnson, A. J. Vogt, and K. F. Kelton, "A structural signature of liquid fragility," Nat. Commun. **5**, 4616 (2014).

[36] C. Zhang, L. Hu, Y. Yue, and J. Mauro, "Fragile-to-strong transition in metallic glass-forming liquids," J. Chem. Phys. **133**, 014508 (2010).

[37] Z. Evenson, T. Schmitt, M. Nicola, I. Gallino, and R. Busch, "High temperature melt viscosity and fragile to strong transition in Zr–Cu–Ni–Al–Nb(Ti) and Cu$_{47}$Ti$_{34}$Zr$_{11}$Ni$_8$ bulk metallic glasses," Acta Mater. **60**, 4712 (2012).

[38] S. M. Chathoth, B. Damaschke, M. M. Koza, and K. Samwer, "Dynamic singularity in multicomponent glass-forming metallic liquids," Phys. Rev. Lett. **101**, 037801 (2008).

[39] H. Okamoto, "Nb–Ti (niobium-titanium)," J. Phase Equilib. **23**, 553 (2002).

[40] J. Brillo, A. I. Pommrich, and A. Meyer, "Relation between self-diffusion and viscosity in dense liquids: New experimental results from electrostatic levitation," Phys. Rev. Lett. **107**, 165902 (2011).

[41] A. Bartsch, K. Rätzke, A. Meyer, and F. Faupel, "Dynamic arrest in multicomponent glass-forming alloys," Phys. Rev. Lett. **104**, 195901 (2010).

[42] I. Gallino and R. Busch, "Relaxation pathways in metallic glasses," JOM **69**, 2171–2177 (2017).

[43] D. Holland-Moritz, F. Yang, J. Gegner, T. Hansen, M. D. Ruiz-Martín, and A. Meyer, "Structural aspects of glass-formation in Ni–Nb melts," J. Appl. Phys. **115**, 203509 (2014).

[44] S. Bogle, P. Voyles, S. Khare, and J. Abelson, "Quantifying nanoscale order in amorphous materials: Simulating fluctuation electron microscopy of amorphous silicon," J. Phys. Condens. Matter **19**, 455204 (2007).

[45] C. Gammer, B. Escher, C. Ebner, A. Minor, H. Karnthaler, J. Eckert, S. Pauly, and C. Rentenberger, "Influence of the Ag concentration on the medium-range order in a CuZrAlAg bulk metallic glass," Sci. Rep. **7**, 44903 (2017).

[46] P. Zhang, J. J. Maldonis, M. Besser, M. Kramer, and P. Voyles, "Medium-range structure and glass forming ability in Zr–Cu–Al bulk metallic glasses," Acta Mater. **109**, 103–114 (2016).

[47] NbS crystal structure: Datasheet from "PAULING FILE multinaries edition – 2022" in SpringerMaterials Springer-Verlag Berlin Heidelberg & Material Phases Data System (MPDS), Switzerland & National Institute for Materials Science (NIMS), Japan, 2023 https://materials.springer.com/isp/crystallographic/docs/sd_0452986.

[48] A. L. Greer, "Confusion by design," Nature **366**, 303–304 (1993).

[49] L. Shadowspeaker, M. Shah, and R. Busch, "On the crystalline equilibrium phases of the Zr$_{57}$Cu$_{15.4}$Ni$_{12.6}$Al$_{10}$Nb$_5$ bulk metallic glass forming alloy," Scr. Mater. **50**, 1035–1038 (2004).

02 June 2024 17:21:06